A comprehensive study on the adsorption-photocatalytic processes using manganese oxide-based magnetic nanocomposite with different morphology as adsorbent-photocatalyst in degradation of azo dyes under UV irradiation

HADIGHEH DORRI[1] ⓘ **, ALI ZERAATKAR MOGHADDAM**[1,*] ⓘ **, EBRAHIM GHIAMATI**[2] ⓘ
and BEHNAM BARIKBIN[2,3] ⓘ

[1] Department of Chemistry, College of Sciences, University of Birjand, 97175-615 Birjand, Iran
[2] Social Determinants of Health Research Center, Birjand University of Medical Sciences, 97175-379 Birjand, Iran
[3] Social Determinants of Health Research Center, Mashhad University of Medical Sciences, 91735-951 Mashhad, Iran
*Author for correspondence (a_zeraatkar_m@birjand.ac.ir)

Abstract. Magnetic MnO_2 nanocomposites with flower-like and wire-like morphologies were synthesized, characterized and well applied for degradation of methyl orange, as model acidic azo dye, from aqueous media. The characterization studies showed the successful formation of the proposed nanocomposites with desirable properties. In addition, the surface properties of the nanocomposite were enhanced by MnO_2 modification, creating more efficient reaction sites for dye degradation. The effects of different factors such as initial pH, dye concentration, contact time, nanocomposite dosage, stirring rate, type and amount of scavenger in degradation efficiency are investigated using experimental design. The degradation efficiencies of nanocomposites with flower-like were higher than its wire-like morphology, and under optimum conditions (i.e., pH 5, catalyst dose 1.5 g l^{-1}, hole scavenger 0.15% (w/v), time 30 min, dye concentration 400 ppm, under stirring rate 300 rpm) degradation efficiencies above 99% were achieved. The kinetics, isotherm and thermodynamic studies for dye degradation process using the proposed nanocomposites were perused. Negative ΔG^o confirms the spontaneous nature of the optical decolourization MO decomposition process. Finally, due to the sample fabrication method, environmental compatibility and good potential due to flower- and wire-like morphologies, the proposed nanocomposites were successfully used as adsorbent-photocatalyst for dye degradation from different real aqueous media.

Keywords. Azo dye; environmental protection; flower- and wire-like morphologies; MnO_2 magnetic nanocomposite; adsorption-photocatalytic degradation.

1. Introduction

Organic contaminants such as dyes, oils, detergents, pesticides, herbicides and pharmaceuticals are more widespread than inorganic contaminants, due to their variety and extent and different applications [1]. Meanwhile, due to the rapid development of textile, pharmaceutical, plastic, leather and petrochemical industries, the emergence of coloured organic compounds is the main cause of pollution of water sources and effluents [2,3]. The textile industry, as one of the most important sources of water pollution, has transferred large amount of dyes to the environment and their presence in aquatic environments [4–6]. In addition to causing toxicity and eutrophication, dyes prevent photosynthesis by disrupting photosynthesis process and resulting in rapid growth of algae and endanger the lives of aquatic organisms and damage the aquatic ecosystem [4–6]. Azo dyes, such as methyl orange (MO) [7], make up about half of the dyes used in the textile industry [6], which are difficult to oxidize and degrade due to their aromatic structure and high solubility in water [1,8]. The persistence for long periods in the environment and the non-destruction of these dyes and their absorption by plants cause genetic mutations and cancer in humans, and have serious effects on human health and the environment [3].

Therefore, the need to remove dye contaminants seems necessary, and it is one of the important tasks in which valuable progress has been made. Many common methods, including physicochemical [9], biological [10], chemical oxidation [11], electrochemical [12] and membrane

filtration processes [13], have been used to remove most organic compounds from dye effluents. These methods are costly, rather nonefficient and the possibility of transferring pollution from one phase to other phase requires more refining processes [2,3]. Advanced processes are required to remove such contaminants, including the use of advanced oxidation technology based on photocatalytic methods and the use of heterogeneous photocatalysts, not only to decolorize and completely degrade and mineralize contaminants, but also as a eco-friendly technology [14], without the presence of any secondary pollution, is effective for the destruction of coloured organic compounds [2,5,15–17]. On the surface of a semiconductor photocatalyst with UV irradiation and the formation of electron–hole pairs, hydroxide ions (OH^-) are oxidized to hydroxide radicals ($OH^\bullet$) in the valence band, and these radicals generated by light can oxidize a wide range of pollutants, including dye pollutants. Superoxide anions are reduced to radicals, which are eventually protonated to produce hydrogen peroxide, that both of which are oxidizing agents [18–20]. Thus, pollutants are converted to water and carbon dioxide as non-toxic substances.

Among the various photocatalytic materials, such as nanofibres, zeolites and metal nanoparticles of palladium, silver, platinum and gold, that are widely used to eliminate inorganic and organic contaminants, manganese oxide is considered as a suitable oxidizer. Manganese oxide is chosen among other metal oxides in heterogeneous processes due to its cost-effectiveness, environmental friendliness and special features, such as ability to prepare different morphological structures, high surface area, low recovery costs, unique crystal structures, and high oxidative degradation potency. Manganese dioxide has more of 20 different polymorphs and polyvalent properties giving them good catalytic properties in removing organic pollutants [4,8,21–24]. Nanoparticles in manganese dioxide, due to high surface energy, tend to accumulate and on the other hand have low resolution. Magnetic fields can prevent mass accumulation due to the high separation efficiency by the external fields, the ease of preparation, and surface modification, in addition to good efficiency in the separation process [1,25]. Cobalt ferrite (CF) is widely regarded as a spinel ferrite due to its excellent magnetic properties at room temperature, and its chemical stability, cost-effectiveness and ease of manufacture [3].

Recently, many studies have been performed on manganese syntheses with different morphologies [26,27]. Since the surface area is a factor affecting catalytic activity, in this study the flower- and wire-like morphologies have been studied, which have a high surface area, high oxidizing ability and good stability in acidic conditions. It can change each structure by controlling the synthesis conditions. So that a combination of the structures of manganese dioxide with the mentioned morphologies in combination with CF magnetic nanoparticles leads to the formation of composite nanostructures, which can be mechanically separated by an external magnetic field [23]. In fact, by controlling the synthesis conditions, each of the morphologies can be displayed with unique properties that are different in terms of shape, structure, size, thermal stability, catalytic and morphological activity [28–30]. We also coated Fe_2O_4 nanoparticles with silica shell for reliable chemical stability, biocompatibility and flexibility in surface modification [31]. Therefore, in this study, we first synthesized CF nanoparticles modified with silica shell (CFS) and then, composite the morphology of the flower and the wire of manganese dioxide to improve its adsorption-photocatalytic properties (Scheme 1). Thus, CFS flower-like MnO_2 (CFSFM) and CFS wire-like MnO_2 (CFSWM) nanocomposites were synthesized and their adsorption-photocatalytic properties in degradation of MO, as model acidic azo dye, in aqueous solution were checked. The treatment procedures were modelled and optimized under response surface methodology. Finally, isotherm, kinetic and thermodynamics of the dye degradation were considered, and the real aqueous samples were treated successfully using the proposed CFSFM and CFSWM.

2. Materials and methods

2.1 *Chemicals*

In order to synthesize the CFSFM and CFSWM nanocomposites, $Fe(NO_3)_3 \cdot 9H_2O$, $Co(NO_3)_2 \cdot 6H_2O$, sodium hydroxide (NaOH), absolute ethanol, ammonium hydroxide, tetraethyl orthosilicate (TEOS ($SiC_8H_{20}O_4$)), $KMnO_4$, $MnSO_4 \cdot H_2O$, $MnCl_2$ and CCl_4 were used. All of these used materials were purchased from Merck Co. (Darmstadt, Germany).

2.2 *Instruments*

The morphological properties of nanoparticles were examined using high-resolution images at different magnifications by transmission electron microscope (TEM) and scanning electron microscope (SEM), using models PHILIPS TM-120 and Quantum 200, USA. The Fourier-transform infrared spectroscopy (FT-IR) analysis was performed to identify the functional groups using a Perkin Elmer FT-IR spectrometer in the range of 400–4000 cm^{-1} by KBr pellets. Changes in the crystal structure of CFSFM and CFSWM nanocomposites during synthesis were performed by the X-ray diffraction (XRD) analysis (Model Philips PW1730 instrument). To identify the elements in CFSFM and CFSWM, the XRF technique, instrument Spectroxepos50, Germany, was used. Also, the Brunauer–Emmett–Teller (BET) analysis, Belsorpmini2 System, Japan, was used. Using the BET, the specific surface area of materials, pore diameter, surface area, volume and size of catalyst pores, adsorption and repulsion isotherms, and pore size
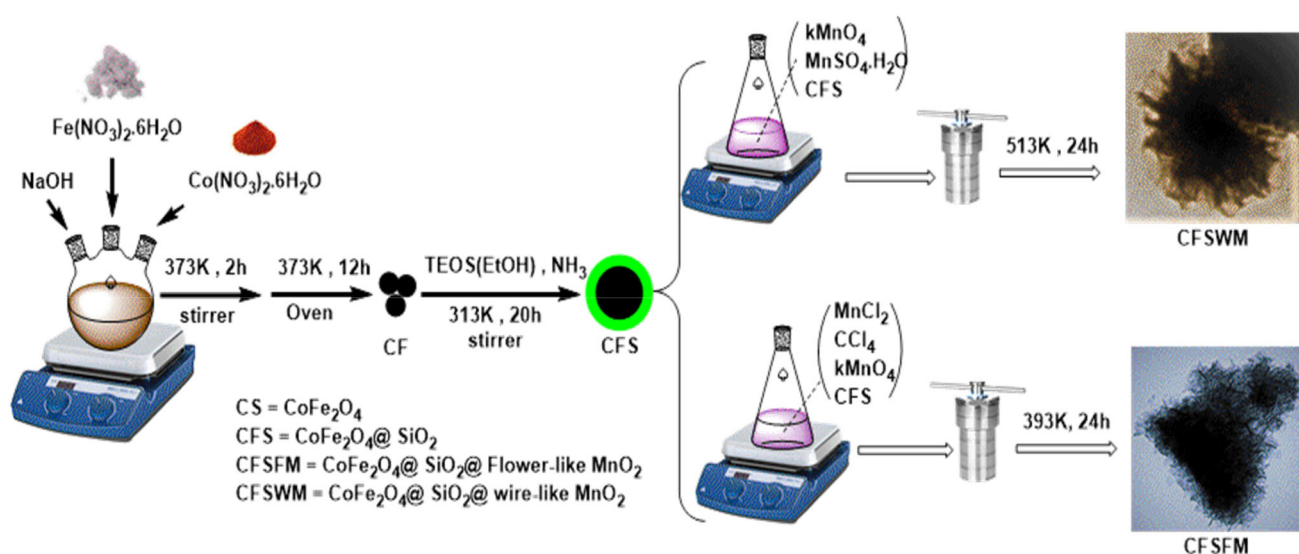
Scheme 1. Preparation of nanocomposites CFSFM and CFSWM.

distribution were analysed. To determine the dye concentration, the UV/Vis spectrophotometer, model T80 from PG Company, England, was used.

2.3 Material synthesis

2.3a *Synthesis of CF nanoparticles:* Synthesis process is illustrated in scheme 1. At first, $Fe(NO_3)_3 \cdot 9H_2O$ and $Co(NO_3)_2 \cdot 6H_2O$ were dissolved in distilled water with Fe^{3+}/Co^{2+} molar ratio of 2:1. The mixture was put into a flask equipped with a mechanical stirrer. A solution containing 1 M NaOH was added dropwise into the mixture under vigorous stirring at 80°C in the oil bath for 2 h. The pH value of the solution reached 14 after the addition of NaOH solution. The resulting nanoparticles were separated from the reaction medium by magnet, and the precipitate was washed by distilled water until the pH value of the solution became neutral. Finally, the resulting precipitate was collected, washed several times with distilled water and then absolute ethanol, and dried at 80°C for 12 h.

2.3b *Synthesis of CFS nanocomposites:* After synthesizing CF, this magnetic core shelled with SiO_2. For this purpose, 25 ml of absolute ethanol was mixed with 6 ml of deionizer water and then 1.5 g of CF nanoparticles were added and sonicated for 30 min to dissolve completely. The flask was put on the magnetic stirrer and 0.8 ml ammonium hydroxide (25 wt%) was added until pH of 12. Then, 0.5 ml of TEOS was mixed dropwise in 10 ml absolute ethanol and allowed to stir for 20 h at room temperature. The resulting brown suspensions were washed repeatedly with double-distilled water and then anhydrous ethanol, and at the end were dried at 80°C for 8 h under

vacuum. After magnetic decantation, CFS core-shell NPs were obtained.

2.3c *CFSFM nanocomposite preparation procedures:* The manganese oxide catalysts were prepared according to the hydrothermal or solution method [26]. Briefly, 30 ml of $MnCl_2$ aqueous solution (1 M) was added to 80 ml of CCl_4 solvent. After stirring for 5 min, 1.16 g CFS nanoparticles were added into the solution and stirred for 5 min, then 40 ml of $KMnO_4$ aqueous solution (0.5 M) was added dropwise. The mixture obtained was filtered, washed three times with deionized water and absolute ethanol, dried under vacuum at 60°C for 24 h. The resulted nanocomposite was used in the next experiments as CFSFM.

2.3d *CFSWM nanocomposite preparation procedures:* A quantity of 1.5 g of $KMnO_4$ and 0.275 g of $MnSO_4 \cdot H_2O$ were mixed in 80 ml of deionized water. Then 1.16 g of CFS was added and mixed for 5 min. After stirring for 0.5 h, the mixed solution was transferred to a 100-ml autoclave for thermal treatment at 240°C for 24 h. The obtained mixture was filtered, washed with deionized water and absolute ethanol, dried at 60°C for 24 h. The resulted nanocomposite was used in the next experiments as CFSWM.

2.4 Proposed procedure for adsorption-photocatalytic dye degradation experiments

The adsorption-photocatalytic process was performed in a 50 ml wide-open glass container. The UV lamp (PHILIPS TUV 15W/G15 T8 made in Holland with the length 43.74 cm and the current of 340 mA) was placed at 2 cm distance from the surface of the containers containing the nanocomposite and MO dye solution. Then, the factors of

pH, initial dye concentration, nanocomposite dosage, stirring speed, contact time, type and amount of hole scavenger (HS) were investigated. For this purpose, first, the pH of MO solution was adjusted by adding HCl and 0.1 M NaOH with a pH metre. Then, appropriate amounts of nanocomposite and HS were added and placed on a stirrer under UV light. The nanocomposite was then isolated by magnetic magnet N42 and then, the concentration of MO was scanned by spectrophotometer in the range of 300–600 nm. In order to conduct isotherm studies, different initial concentrations of MO were changed. To study reaction kinetics, different contact times, and for thermodynamics investigation at different temperatures were checked while other factors were kept in optimal condition. The values of adsorption-photocatalytic degradation efficiency (DD), adsorption capacity (q_e), and equilibrium capacity (q_t) at time t were obtained by the following equations:

$$DD(\%) = \left(\frac{C_0 - C_t}{C_0}\right) \times 100 \qquad (1)$$

$$q_e = \frac{(C_0 - C_e) \times V}{m} \qquad (2)$$

$$q_t = \frac{(C_0 - C_t) \times V}{m} \qquad (3)$$

where C_0, C_e and C_t (mg l^{-1}) are MO concentration at first, equilibrium and any arbitrary time (t), respectively. Also, m (g) is the mass of the used CFSFM and CFSWM and V (l) is the solution volume.

2.5 Modelling methodology

First, the effective factors in the MO decolorization process based on preliminary studies and experiments were selected, and while the temperature was kept constant at room temperature, the samples were exposed to UV irradiation. Modelling and optimization were performed with the central composite design (CCD) using the trial version of Design Expert 11.0.0 package (Stat-Ease Inc., Minneapolis, MN, USA).

3. Results and discussion

3.1 Characterization of CFSFM and CFSWM nanocomposites

3.1a *SEM and TEM analysis:* Using SEM, the surface of the sample was scanned. The images of the samples and their surface topography are shown in figure 1. As shown in figure 1a and b, CFSFM nanocomposite that was prepared by hydrothermal method with CCl$_4$ solution at 120°C had morphology sphere-like [23], while CFSWM nanoparticle that was prepared with the hydrothermal method at 240°C for 24 h had a wire-like morphology [18]. In other words,

with the long-term hydrothermal process, the morphology of the structure changes to the wire. From these images, it can be seen that CFSWM nanoparticles are uniformly distributed on the CFS surface after the hydrothermal process. In other words, this type of morphology with a high specific surface area can facilitate the intercalation process of soluble ions. Figure 1c and d shows TEM from the inside structure of the samples. TEM images show a wire-like structure with a smooth surface for CFSWM. High-resolution images confirm MnO$_2$ wire coverage on CFS.

Also, figures show the TEM image of the particle in which the configuration of the shell and its core with dark nuclei and grey shells is related to mass densities different from CF, SiO$_2$ and MnO$_2$ [24,32]. Since CF has superparamagnetic properties, it also maintains its crystalline properties at low temperatures; SiO$_2$ shells not only protect the CF core from degradation in harsh environments, especially acidic environments, but also provide surfaces compatible with many reactions and compounds due to their easy surface modification. It can be seen that the difference in the preparation method leads to a large difference in the level of catalysts with a similar crystal structure. CFSFM nanoparticles have a spherical morphology with a uniform floral architecture. These structures are also composed of hierarchical microsphere/nanoplates structure. The nanostructures have grown perpendicular to the centre of the crust. TEM images also show that the synthesized CFSFM composite contains a layer of manganese dioxide whose surface morphology has changed to a hierarchical flower-like structure.

3.1b *XRF analysis:* In order to quantitatively analyse and identify the composition of elements in CFSFM and CFSWM nanocomposites, X-ray fluorescence was used qualitatively and quantitatively. The main components of synthesized nanocomposites based on the weight percentage of elements and their constituents according to ASTM E1621(2013) test reference standard and sample L.O.I. at 900°C temperatures are as in table 1.

As shown in table 1 of chemical composition, the main components of CFSFM and CFSWM nanocomposites are related to manganese and iron with values of 74.34 and 8.72% for CFSFM, and 48.81 and 15.82% for CFSWM, respectively. Higher weight percentages of manganese for CFSFM indicate a wider morphology with a higher level in its synthesis method. The decrease in Mn and the increase in Fe, Co, Si in CFSWM compared to CFSFM indicate the relationship between the composition and thickness of the coating layers of Si and MnO$_2$ in its different structures, and confirm that the thickness of the manganese dioxide layer in CFSFM catalyst is greater than CFSWM.

3.1c *XRD analysis:* In order to investigate the crystal structure and determine the phase of CFSFM and CFSWM nanocomposites based on XRD, the XRD spectrum of the
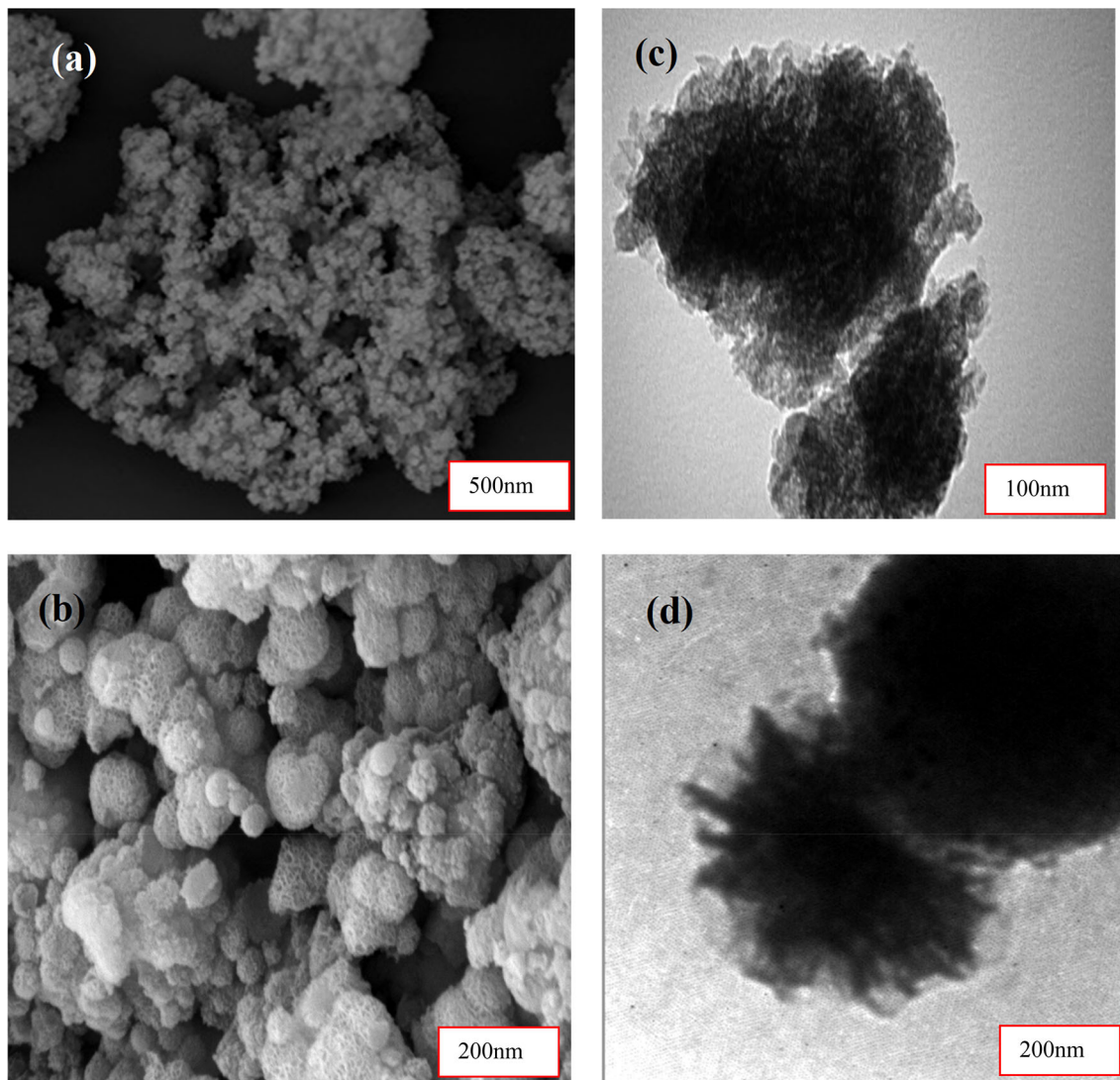
Figure 1. (**a**, **b**) SEM and (**c**, **d**) TEM images of CFSFM and CFSWM, respectively.

Table 1. X-ray fluorescence spectroscopy of CFSFM and CFSWM samples, based on the weight percentage of elements and constituents.

	Al (wt%)	Si (wt%)	K (wt%)	Mn (wt%)	Fe (wt%)	Co (wt%)
CFSFM	1.63	7.71	3.21	74.34	8.72	4.38
CFSWM	0.68	12.58	13.68	48.81	15.82	8.43

JCPDS No. 10-0325 reference bank was used. The synthesized CFSFM diffraction peaks appeared at 18.25, 30.31, 35.82, 36.93, 41.53, 57.34, 62.92 and 63.97°, while the CFSWM diffraction peaks were at 12.30, 30.60, 36.03, 43.65, 53.91, 57.68, 63.50 and 65.83° corresponding to (1 1 1), (2 2 0), (3 1 1), (2 2 2), (4 0 0), (4 2 2), (5 1 1) and (4 4 0). As can be seen, the peaks of CFSFM and CFSWM are recorded at almost the same angles and the peak angles are well-matched to each other. However, as shown in figure 2, the peak intensities in CFSWM are higher than in CFSFM, it can be concluded that the plate spacing in CFSWM is probably longer than in CFSFM. Since the CFSFM peaks are wider and less intense, the particle size of the CFSFM material is smaller. In addition to microstructural changes that have affected the intensity of the width of XRD peaks, trelliswork strains and grain size have also been reported as a propagation factor in the Williamson–Hall model. In this way, the intra-network strains reduce or
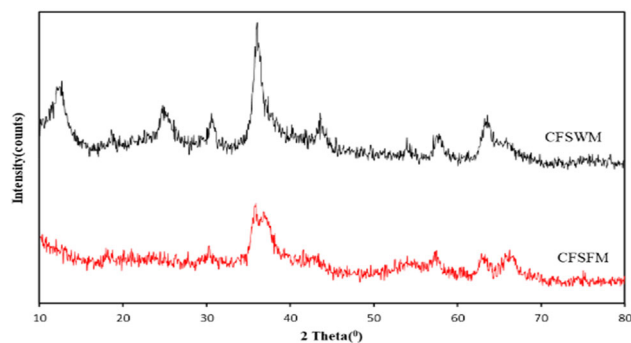
Figure 2. The XRD pattern of synthesized CFSFM and CSFWM.

increase the distance between the crystal plates and thus lead to the flattening of the peaks. There is also no other characteristic peak due to the presence of impurities in the synthesized samples, which indicates the purity of the synthesized samples is high and it can be concluded that the coating of SiO_2 and MnO_2 layers do not cause a phase change in the structure of nanoparticles [33]. Also, since increasing the temperature accelerates the process of nucleation within the cell and the crystallization of nanoparticles occurs faster at higher temperatures, probably with increasing the synthesis temperature of CFSWM nanocomposite, its crystal size increases and the relative crystallinity of the product is increased.

3.1d   *BET analysis:*   BET analysis is a physical analysis method based on the adsorption and desorption of gas molecules on a solid surface, in order to analyse the structure of porous materials, especially catalyst-based materials. This technique is also useful to investigate the specific surface size of catalysts and nano-adsorbents, the particles average size, porosity, shape and size of porosity [34]. The N_2 adsorption and desorption curves for CFSFM and CFSWM are shown in figure 3. Based on this, the average dimensions of pores for CFSFM and CFSWM were obtained as 10.492 and 24.555 nm, respectively. Also based on the calculations of BET, the amount of specific surface area and total particle size for CFSFM and CFSWM were 57.107 $m^2 g^{-1}$,   0.1498 $cm^3 g^{-1}$ and   7.5829 $m^2 g^{-1}$, 0.04654 $cm^3 g^{-1}$, respectively. As shown in the CFSFM figure, the hysteresis loop in the relative pressure range of 0.3–1 represents an isotherm of type IV, which is related to the mesoporous material. Their most important characteristic is the loop hysteresis, which is related to the condensate of the cavities [35]. While in the same pressure range, CFSWM represents the reversible isotherm of type III. In this type, the graph of the amount of adsorption in terms of relative pressure is convex, which in fact shows a relatively weak interaction between adsorbent and adsorbate and the interaction between adsorbate and adsorbate that play a very important role.

However, in this case, the structure is not porous and their strength is very weak. This type of isotherm includes adsorption of the single layer at low pressure and adsorption of multilayer at high pressure. They are meso-cavities and due to the hysteresis of the presented materials, the estimated cavities of the cavities related to CFSFM and CFSWM are slits and cylindrical, respectively. Using BJH theory, the volume and area distribution of cavities and the diameter of cavities for mesoporous materials can be obtained. According to the distribution diagram, the size of the holes is in the range of 1–100 nm and represents a narrow peak with a centre of 1.85 nm for CFSFM and 12.244 nm for CFSWM. Based on the above, to determine the performance of CFSFM and CFSWM catalysts, the specific surface area for CFSFM is larger than CFSWM, which interacts more with the reactants and improves mass transfer. Also, due to the magnetic properties of the synthesized nanocomposites, the higher specific surface area catalyst separation will be easier and the chances of adsorption-photocatalytic activity will increase.

3.1e   *FTIR analysis:*   The FT-IR spectra of the mesoporous catalyst in figure 4 are very consistent with the XRD results. IR vibration bands at 526, 528, 579 and 622 cm^{-1} can be used to vibrate Mn-O, Co-O and Fe-O of the structure, and the band at 1428, 1400, 1637 and 1110 cm^{-1} might suggest plausible Mn-OH bonds. The bands of about 1629 and 3409 cm^{-1} were attributed for the stretching vibrations of the inner hydroxyl group and inner surface hydroxyl group [36,37]. Peaks 570, 802 and 1098 cm^{-1} are related to the asymmetrical stretching of Fe-O-Fe, asymmetric tensile oscillation of Si-O-Si and symmetric tensile oscillation of Si-O-Si, respectively [38]. Wide peak of 3300–3600 cm^{-1} is related to stretching vibration of Si-OH, and confirms the formation of silica coating on iron oxide core in the second stage of synthesis. Additionally, the representative peak for Co-O-Si and Fe-O-Si binding presented between the CF and SiO_2/MnO_2, which was supposed to be at around 584 cm^{-1}, was overlapped by the band of Co-O and Fe-O of CF nanoparticles. Finally, the expected characteristic absorption peaks in the spectra were consistent with the XRD results. The above results, in addition to confirming the conclusion of XRD, also verified the success of functionalization of the final product CFSFM and CSFWM.

3.2   *Experimental design*

After conducting preliminary studies and experiments, to determine the effective factors and their effect on the adsorption-photocatalytic dye degradation process, design expert software was used to screening, modelling and optimizing the conditions. Initially, the fractional factorial design (FFD) screening method was used to select the factors affecting the process, and then optimization was performed on the selected factors.
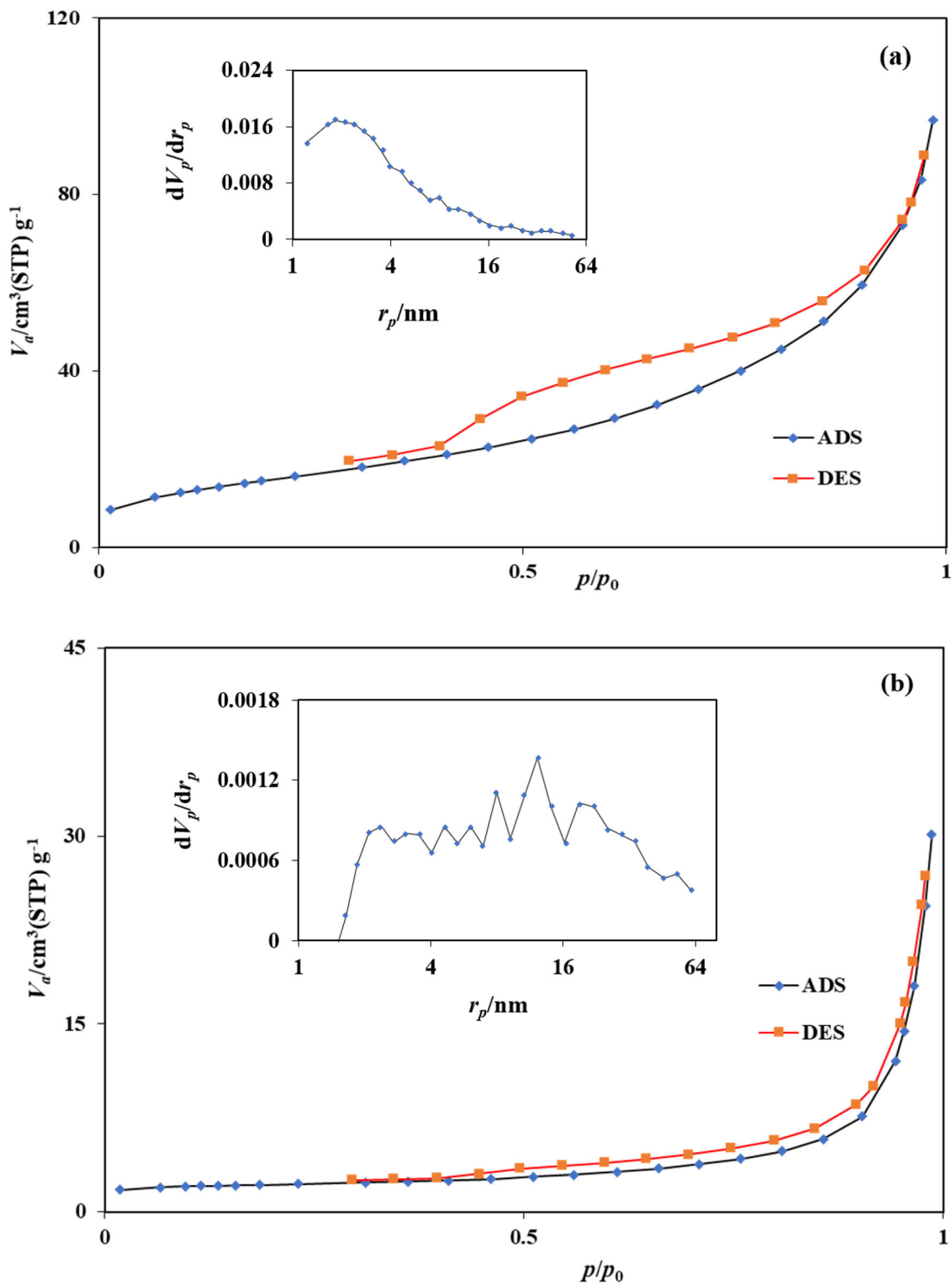
Figure 3. N$_2$ adsorption/desorption isotherms, pore size distributions of catalysts, BJH plot of (**a**) CFSFM and (**b**) CFSWM.

Based on the initial experiments for CFSFM nanocomposite, the following factors were selected: 6 main factors, i.e., pH, contact time, nanocomposite dose, initial concentration, speed and amount HS. For CFSWM nanocomposite, 5 main factors, i.e., pH, contact time, initial concentration, speed and amount HS that affects the efficiency of decolorization were selected. Room temperature and UV irradiation conditions were kept constant during degradation

Figure 4. FTIR spectra of CFSFM and CFSWM.

process. We use the Pareto diagram to show the effective factors in the process. Based on this diagram, important and effective factors were selected for a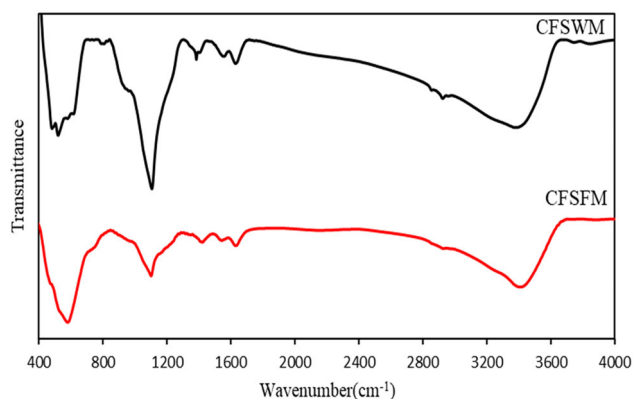dsorption-photocatalytic decolorization. For development in the evaluated process, CCD-based RSM was used as an experimental design to optimize adsorption-photocatalytic decolorization of dye instead of the one-time factor (OAT) method. RSM is an efficient and cost-effective statistical method to investigate the effect of various factors on processes. The purpose of designing the experiment with the response surface method is to optimize the output variable while it is affected by several independent variables. Among its advantages is the need for less time and experiments, as a result of reducing costs and the possibility of studying the interaction and interaction of independent factors on the response to achieve the highest impact factor that is consistent with statistical work. Therefore, we used CCD composite design, which is a tool for quadratic design [39], and on the other hand, after the screening stage, this nonlinear model was used because curvature became important. In the CCD modelling stage, a total of 90 runs were performed for the CFSFM to investigate the effect of sample pH (A; 2–5), the sorbent weight to sample volume ratio (B; 0.5–1.8 mg ml^{-1}), contact time (C; 3.6–11.4 min), initial concentration of MO (D; 200–456 ppm) and amount HS (E; 0.07–0.23 %v/v) and speed (F; 143–456 rpm). A total of 54 runs were performed for the CFSWM to investigate the effect of sample pH (A; 1.6–6.4), contact time (B; 1.5–13.5 min), initial concentration of MO (C; 62.2–537.8 ppm), amount HS (D; 0.03–0.27 %v/v) and speed (F; 62–538 rpm). Two other factors, i.e., temperature at 25 C and UV intensity were kept constant during the adsorption-photocatalytic decolorization. In order to determine the number of design points required (N) in CCD for k parameters, the following equation was used:

$$N = 2^k + 2k + N_o \qquad (4)$$

where N_o and k are the number of replicates in the design centres as well as the number of parameters [40]. According to the above equation, the required experiments for CFSFM were performed in five blocks and CFSWM nanocomposite

was done in three blocks. The appropriate range for the studied parameters was based on the preliminary experiments.

3.2a *ANOVA analysis:* The data obtained from adsorption-photocatalytic decolorization were analysed by the proposed method based on analysis of variance (ANOVA), the results of which are given in tables 2 and 3. According to the data in the tables, the F-value of the model for CFSFM and CSFWM is 47.40 and 183.42, respectively. These values indicate the significance of the model and a proof of the importance of the proposed model and the probability that the values of reduction efficiency obtained is very low due to noise. Based on the calculated value of F-value for each factor, the significance of the effect on the response has been confirmed. To determine the significance of the model and the effect of each parameter, the F-value and *p*-value were used.

The *p*-value ($p < 0.05$) is significant and if its value is less than 0.001 it indicates the significant effect of the parameter. The higher value of F for a parameter represents the greater effect on that parameter in the process [41]. According to ANOVA table, initial concentration parameter of MO with F-value = 160 and 96.66 is the most effective factor for decolorization with CFSFM and CSFWM, respectively. Also, the pH is important in the next categories for the studied nanocomposites. As shown in the ANOVA table, since the mean squares of the models are high, the model covers a large portion of the data and is a reliable model. The lock of fit *p*-values for CFSFM and CFSWM were 0.1750 and 0.9822, respectively ($p \geq 0.05$), which indicates that non-fits are not important [42].

The degree of conformity of the model on the data of each response was evaluated with coefficient of determination (R^2), adjusted coefficient of determination (R^2_{adj}) and coefficient of predictive determination ($R^2_{predict}$). The adjusted coefficient of determination is the value of the coefficient that is set for a larger number of factors in the model and is used to evaluate the model [43]. The predicted coefficient of determination is used to estimate the power of the regression model in predicting new observations and prevents higher estimates than the values fitted with the model. As can be seen, the regression model has a high regression coefficient for both cases and the value of R^2 indicates the importance of the model. Regarding R^2_{adj}, it seems that there is no significant difference between R^2 and R^2_{adj}. Also, the value of adequate precision, as a criterion of signal/noise ratio at value >4, is more than 4 [44]. Therefore, the ratio of 22.56 for CFSFM and 49.67 for CFSWM indicates the appropriateness of the model. Based on the coded equations, it can be used to identify the relative influence of factors influencing the response by comparing coefficients. The parameters with a positive sign indicate a synergistic effect and a negative sign indicate a decreasing effect.

Table 2. ANOVA for quadratic model for decolorization efficiency of MO by CFSFM.

Source	SS[a]	MS[b]	DF[c]	F-value	p value
Model	1.786×10^{12}	6.616×10^{10}	27	22.37	< 0.0001
A: sample pH	2.983×10^{11}	2.983×10^{11}	1	100.84	< 0.0001
B: dose	3.560×10^{11}	3.560×10^{11}	1	120.35	< 0.0001
C: contact time	1.163×10^{9}	1.163×10^{9}	1	0.3932	0.5332
D: initial concentration	4.010×10^{11}	4.010×10^{11}	1	135.54	< 0.0001
E: HS amount	2.902×10^{9}	2.902×10^{9}	1	0.9809	0.3262
F: speed	1.249×10^{9}	1.249×10^{9}	1	0.4222	0.5185
AB	1.176×10^{11}	1.176×10^{11}	1	39.74	< 0.0001
AC	2.704×10^{8}	2.704×10^{8}	1	0.0914	0.7635
AD	1.374×10^{11}	1.374×10^{11}	1	46.43	< 0.0001
AE	6.843×10^{8}	6.843×10^{8}	1	0.2313	0.6324
AF	2.301×10^{8}	2.301×10^{8}	1	0.0778	0.7814
BC	7.505×10^{7}	7.505×10^{7}	1	0.0254	0.8740
BD	3.168×10^{11}	3.168×10^{11}	1	107.10	< 0.0001
BE	1.858×10^{9}	1.858×10^{9}	1	0.6281	0.4314
BF	1.934×10^{8}	1.934×10^{8}	1	0.0654	0.7991
CD	3.081×107	3.081×10^{7}	1	0.0104	0.9191
CE	4.540×107	4.540×10^{7}	1	0.0153	0.9019
CF	4.145×107	4.145×10^{7}	1	0.0140	0.9062
DE	3.385×10^{8}	3.385×10^{8}	1	0.1144	0.7364
DF	2.676×10^{8}	2.676×10^{8}	1	0.0905	0.7647
EF	7.149×10^{8}	7.149×10^{8}	1	0.2416	0.6249
A^2	1.056×10^{11}	1.056×10^{11}	1	35.69	< 0.0001
B^2	4.215×10^{10}	4.215×10^{10}	1	14.25	0.0004
C^2	1.634×10^{10}	1.634×10^{10}	1	5.52	0.0223
D^2	2.169×10^{10}	2.169×10^{10}	1	7.33	0.0090
E^2	1.487×10^{10}	1.487×10^{10}	1	5.03	0.0290
F^2	2.433×10^{10}	2.433×10^{10}	1	8.23	0.0058
Residual	1.657×10^{11}	2.958×10^{9}	56		
Lack of fit	1.568×10^{11}	3.336×10^{9}	47	3.38	0.0275
Pure error	8.877×10^{9}	9.863×10^{8}	9		
Cor total	2.284×10^{12}		87		
Std. dev.	50060.40	R^2	0.9127	Adeq precision	22.5639
Mean	8.407E+05	Adjusted R^2	0.8934		
CV %	5.95	Predicted R^2	0.8448		

[a]Sum of square.
[b]Mean square.
[c]Degree of freedom.

Equations 5 and 6, in terms of coded parameter:

$(\text{DD by CFSFM})^3$

$$
\begin{aligned}
= {} & (7.7 \times 10^5) + 68272.6A + 71770.5B + 4109.7C \\
& - 76286.2D - 6479.2E + 4256.6F - 42857.9AB \\
& + 46326.4AD + 70357.7BD + (3.6 \times 10^5)A^2 \\
& - 65484.3B^2 - 42885.8C^2 - 49100.8D^2 - 38887.4E^2 \\
& - 51673.6F^2
\end{aligned}
\tag{5}
$$

$$
\begin{aligned}
(\text{DD by CFSWM}) = {} & 78.67 + 0.41A + 0.11B - 1.44C \\
& + 0.13D + 0.33E + 0.35CE \\
& + 5.36A^2 - 1.28B^2 - 2.64C^2 \\
& - 2.05D^2 - 2.83E^2
\end{aligned}
\tag{6}
$$

According to the model, pH, dosage, contact time and speed (a positive effect) and HS, MO initial concentration (a negative effect) by CFSFM nanocomposite, and HS, contact time and speed (a positive effect) and pH, MO initial concentration (a negative effect) by CFSFM nanocomposite have the greatest effect on efficiency of degradation process, respectively.

3.2b *Model adequacy:* To investigate the validity of the proposed model, the normal distribution curve was used (supplementary figures S1a and S2a). The normal distribution curves for CFSFM and CFSWM represent the natural error values for both nanocomposites, and the residual curve follows the normal distribution. To be sufficient for the model, a residual diagram (supplementary figures S1b and

Table 3. ANOVA for quadratic model for decolorization efficiency of MO by CFSWM.

Source	SS	MS	DF	F-value	p value
Model	1889.15	94.46	20	90.56	< 0.0001
A: sample pH	7.41	7.41	1	7.11	0.0130
B: contact time	0.5033	0.5033	1	0.4825	0.4934
C: initial concentration	90.24	90.24	1	86.52	< 0.0001
D: HS amount	0.7944	0.7944	1	0.7617	0.3908
E: speed	4.80	4.80	1	4.60	0.0415
AB	0.0012	0.0012	1	0.0012	0.9726
AC	2.20	2.20	1	2.11	0.1579
AD	0.2112	0.2112	1	0.2025	0.6564
AE	0.0113	0.0113	1	0.0108	0.9181
BC	0.5000	0.5000	1	0.4794	0.4948
BD	0.6612	0.6612	1	0.6340	0.4331
BE	0.0112	0.0112	1	0.0108	0.9181
CD	0.2450	0.2450	1	0.2349	0.6320
CE	3.92	3.92	1	3.76	0.0635
DE	1.71	1.71	1	1.64	0.2115
A^2	1511.11	1511.11	1	1448.81	< 0.0001
B^2	85.82	85.82	1	82.28	< 0.0001
C^2	357.02	357.02	1	342.30	< 0.0001
D^2	221.14	221.14	1	212.02	< 0.0001
E^2	411.26	411.26	1	394.30	< 0.0001
Residual	27.12	1.04	26		
Lack of fit	15.58	0.7420	21	0.3216	0.9704
Pure error	11.54	2.31	5		
Cor total	3042.74		48		
Std. dev.	0.9662	R^2	0.9829	Adeq precision	49.6732
Mean	93.35	Adjusted R^2	0.9776		
CV %	1.04	Predicted R^2	0.9588		

S2b) is used to show that the data distribution does not follow a specific trend and variance between the data are fixed and show the independency of data.

The diagram of real prediction values shows the efficiency of the proposed model in predicting the adsorption-photocatalytic decolorization efficiency of the proposed substrates. For adequacy of the model, the residual diagram shows the independent hypothesis and/or the variances are constant in the design of the CCD model according to the predicted values, and the obtained points do not follow a specific pattern. According to *BOX-COX* diagrams (supplementary figures S1c and S2c), to distribute specific errors, there is no need for transformation. According to the *Cook's* diagram (supplementary figures S1d and S2d), we do not need to modify the model, and in fact, it is an expression of outlier data and considers the relationship with the response.

3.3 *Effect of operational parameters on dye degradation using CFSFM/CFSWM nanocomposites under simulated sunlight irradiation*

Using contour and three-dimensional curves (figures 5 and 6), the effect of different factors on the efficiency of MO

adsorption-photocatalytic decolorization process was investigated by the proposed substrates [45]. The obtained results from the effect of the studied parameters show that all the mentioned parameters have a significant effect on the adsorption-photocatalytic activity of the synthesized nanocomposites. Also, according to the results of ANOVA both CFSFM and CFSWM substrates, and dye concentration have the greatest impact on the decolorization process.

3.3a *Effect of irradiation time and contact time:* With increasing irradiation time and contact time, the adsorption-photocatalytic activity of nanocomposites increased significantly, so that the maximum decolorization of CFSFM nanocomposite was achieved in 7.5 min and CFSWM in 10 min. This time may be due to differences in the gap band of this type of substrate. As, for excitation of the electron–hole pair for CFSFM requires more UV light and a higher gap band, and is excited later than CFSWM nanoparticles with shorter gap bands. Therefore, at the same time, CFSFM nanoparticles have more electrical excitation and produce more electron pair holes, which lead to the production of more hydroxyl oxidizing radicals.

Therefore, when UV irradiated, CFSFM nanoparticles are able to further degrade MO. The dose–time diagram shows
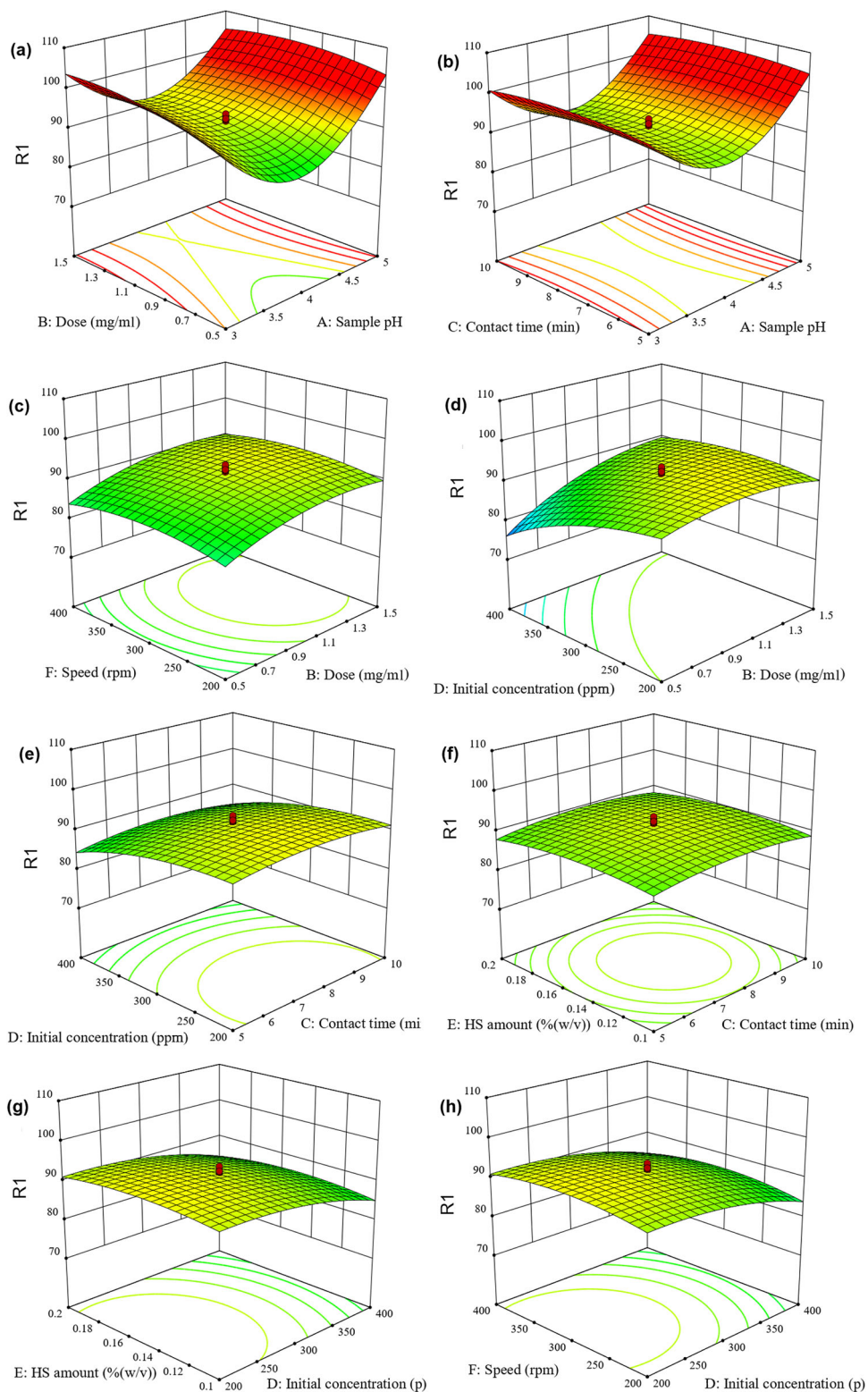
Figure 5. The wireframe plots of CFSFM, (**a**) the nanocomposite dosage and solution pH, (**b**) contact time and solution pH, (**c**) nanocomposite dosage and speed, (**d**) MO initial concentration and nanocomposite dosage, (**e**) contact time and MO initial concentration, (**f**) contact time and HS amount, (**g**) the HS and MO initial concentration, (**h**) MO initial concentration and speed, on MO adsorption-photocatalytic decolorization efficiency.
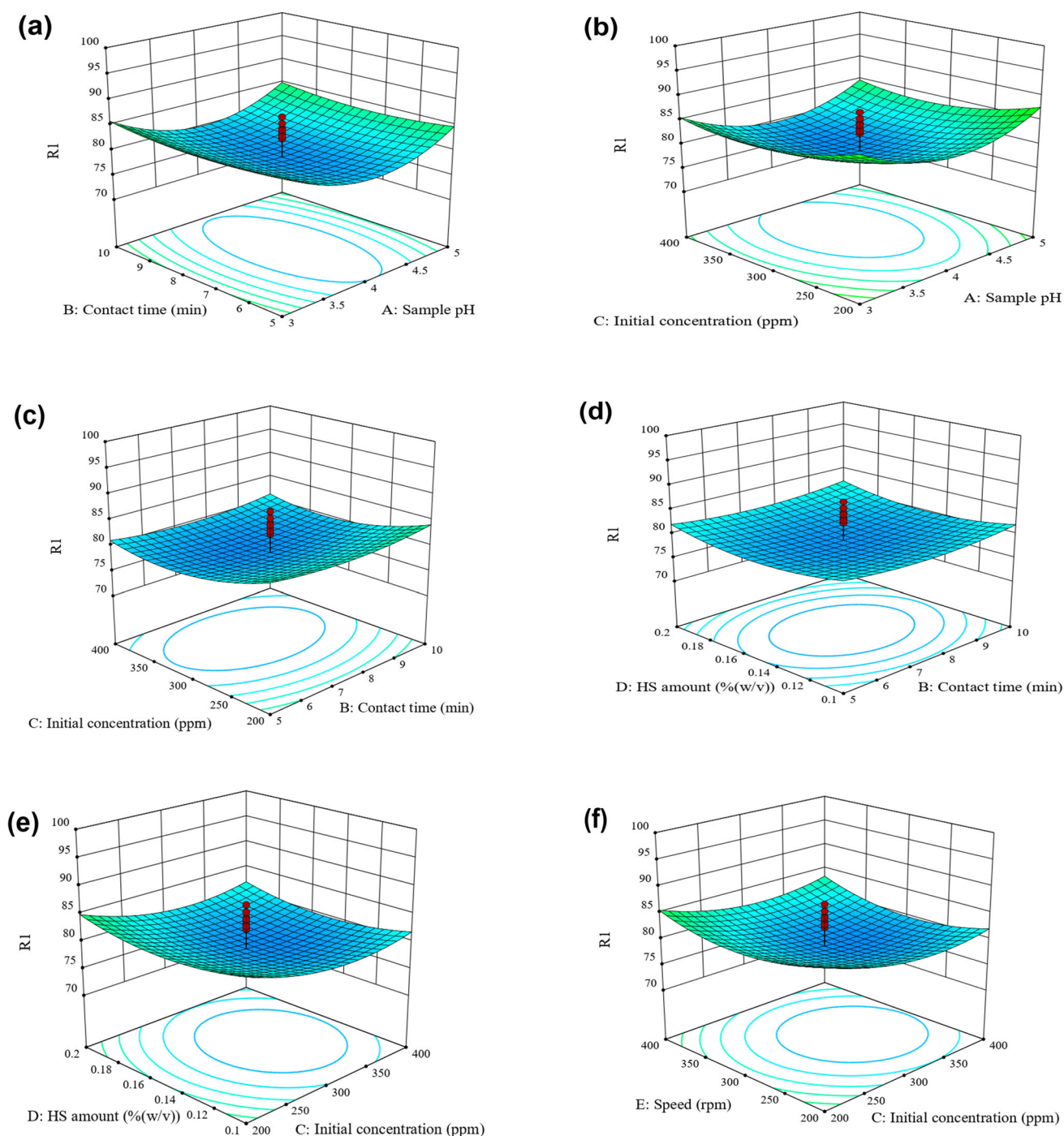
Figure 6. The wireframe plots of CFSWM, (**a**) contact time and solution pH, (**b**) MO initial concentration and solution pH, (**c**) MO initial concentration and contact time, (**d**) contact time and HS amount, (**e**) HS amount and MO initial concentration, (**f**) MO initial concentration and speed, on MO decolorization efficiency.

the greater impact of time on the decolorization efficiency. Because with increasing time, the amount of electron excitation increases much, and as a result, the pair of electrons in the production hole is increased which causes the oxidation and decomposition of the pollutant per unit volume. The highest adsorption-photocatalytic decolorization and degradation efficiencies for CFSFM and CFSWM

can be described as having sufficient opportunity to produce more free radicals and their contact with the dye.

3.3b *Effect of nanoparticle type and catalyst dosage:* Particle size is a very important factor in adsorption-photocatalytic activity, because it directly affects the specific surface area of the catalyst. In general,
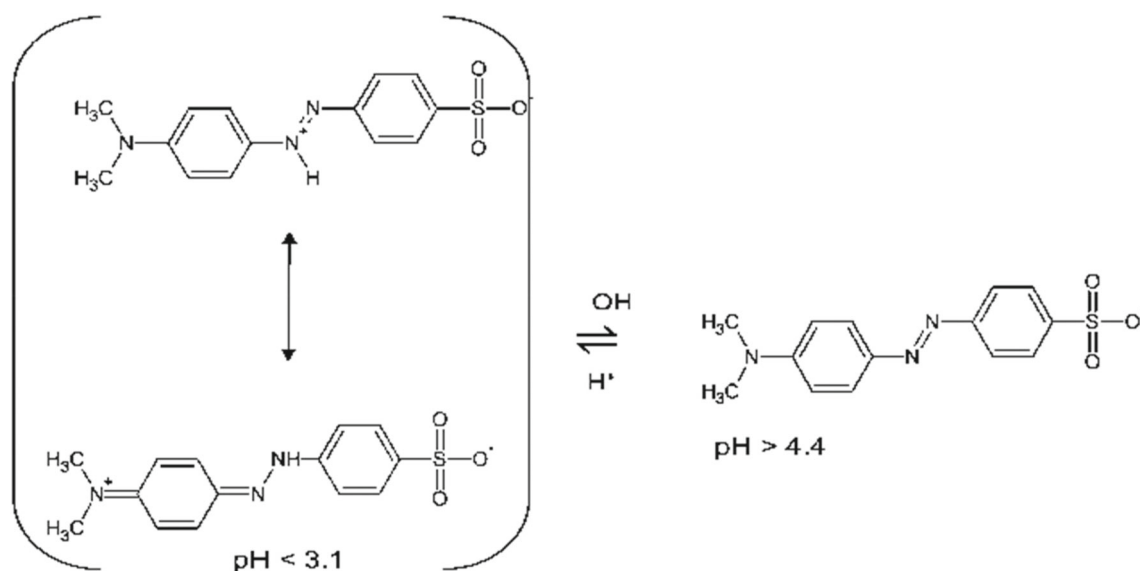
Figure 7. The molecular structure of MO in different pH solutions.

the smaller the particle size, the larger the specific surface area, and the higher the activity is expected because the number of active sites per square metre is increased. Thus, the transfer rate of surface charge carriers will be increased and the amount of contaminant adsorption on the catalyst surface will be higher.

Thus, by reducing the particle size to a critical size, the adsorption-photocatalytic activity is increased and when the particle size is decreased to less than the critical size, the adsorption-photocatalytic activity is decreased. Increasing the dose can be attributed to the increase in the number of electron pairs in the cavity and thus, to the oxidizing produced radical due to the increase in the amount of nanocomposite. Also, with increasing the amount of nanocomposite due to the increase of active sites for the production of free radicals and the reaction of degradation of dye molecules, the rate of adsorption-photocatalytic decolorization is increased. For CFSFM, the optimal conditions were obtained at 1.5 mg ml^{-1}, and for CFSWM the optimal conditions were obtained at 1 mg ml^{-1}. Due to the smaller surface area in CFSWM, more time is needed to complete the process than in CFSFM. Also, oxygen produced by UV light is used for MO oxidation until the minerals are fully produced. The efficiency is increased by increasing the dose to 1 mg ml^{-1} for CFSWM. By increasing the catalyst more than the optimum amount, it causes the accumulation of particles and reduces the number of surfactants. On the other hand, an excessive increase of the catalyst causes turbidity of the solution and reduction of light transmission and reduces the value of adsorption-photocatalytic decolorization. In fact, the highest percentage of MO decolorization with nanocomposite doses of 1.5 mg ml^{-1} for CFSFM and 1 mg ml^{-1} for CFSWM is related to the production of more oxidizing species.

3.3c *Effect of MO initial concentration:* As the nanocomposite dose is increased, the number of free sites for adsorption is increased until all dye molecules adsorb the active sites on the surface of the nanocomposite. Increasing the nanocomposite while maintaining the dye concentration increases the free surface area for adsorption-photocatalytic decolorization and MO degradation. At low concentrations of MO, the present amount of active and radical sites is sufficient to adsorb all MO molecules and degrade the dye through photocatalytic oxidation. However, with increasing concentration of MO in solution, the decolorization process decreases due to adsorption of limited sites. Moreover, the continuous production of OH radicals is insufficient for the complete destruction of all dye molecules. In fact, by increasing the MO concentration, the path length of UV input photons to the dye solution is decreased to stimulate the nanomaterial surface [46]. Also, at high concentrations, the lack of direct contact between MO molecules and the adsorbent-photocatalyst surface stops adsorption-photocatalytic activity due to increased mass resistance and the production of fewer active species on the surface. In addition, increasing the concentration can increase the production of formed intermediates and attach to the catalyst, and thus reduce the destruction efficiency [47].

3.3d *Effect of pH::* The decolorization process is strongly dependent on pH [5]. Since pH changes the surface of the nanocomposite, it plays an important role, especially in the adsorption capacity, which is caused by the adsorbent surface charge, the amount of ionization of materials in solution as well as the separation of functional groups in the degradation sites. Since MO is an anionic dye; the electrostatic attraction between the adsorbent and the dye is the main factor in increasing the adsorption capacity under acidic conditions [40]. At high pH, the decolorization action is not desirable due to the presence of electrostatic repulsion force between anionic dye molecules and negatively charged sites on the adsorbent surface. Because at alkaline pHs, the production of hydroxide functional groups in the environment is increased, which

causes a negative electric charge on the nanocomposite surface. Therefore, weak interaction or even repulsive force between the dye and the surface of the nanocomposite reduces the degradation.

Low pH values lead to a positive charge on the nanocomposite surface, so the adsorption of MO anions (figure 7) to the surface is increased and leads to an increase in adsorption-photocatalytic degradation efficiency. Increasing the pH from acidic to alkaline conditions leads to electrostatic repulsion between MO anions. The nanocomposite surface hydroxyl anions are deposited on the catalyst. In addition, in alkaline conditions, adsorption of OH^- on the nanocomposite surface leads to a reduction of the decolorization process at high pH values. The acidic and alkaline form of MO indicates that with increasing acidity of the solution, the colour of MO changes from yellow to orange and with a change in pH from 4 to 3 changes to red.

3.3e *Effect of formic acid as HS:* Another way to enhance the photocatalytic performance, in addition to modifying catalysts, is to add sacrificial electron donors to the reaction system. One of the problems of the adsorption-photocatalytic reaction is the electron–hole recombination, which drastically reduces the efficiency of the reaction. To solve this problem, electron acceptor materials, such as HS, must be added to the reaction system. Distinct types of sacrificial reagents (HS) are commonly found that have different effects on different systems. Therefore, selecting a suitable and effective HS is especially important for improving catalytic performance. In this study, based on preliminary experiments in the presence of different hole scavenger and similar studies, formic acid with a simple molecular structure of carbon was selected as the perforation to investigate its effect on the degradation of methyl orange dye. The binding of formic acid to the surface of manganese dioxide, its simple oxidation to carbon dioxide, the production of minimal intermediates, the ability of pair anions to inhibit hydroxyl radicals, the formation of highly reducing radicals and the facilitation of mineralization were among the reasons for selecting formic acid [48–50]. The oxygen in HS reacts with the electron and prevents electron–hole recombination. It also generates free radicals in ultraviolet radiation, which play a key role in the adsorption-photocatalytic process [4].
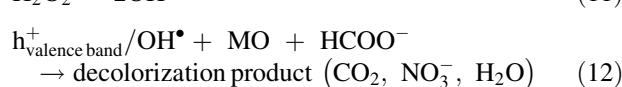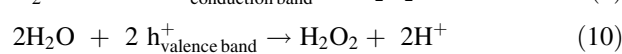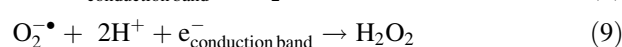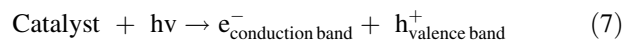
Load changes are likely to prevent further load changes on the surface, as the surface of the CFSFM layer is thicker and larger than the CFSWM layer.

The maximum decolorization rate was obtained with the presence of 0.15% (v/v) formic acid for CFSFM and 0.2% formic acid for CFSWM. With increase in HS concentration, the process is decreased more than the optimal value. Because by increasing the concentration of formic acid more than the optimal amount, this substance decomposes into oxygen and water, and hydroxyl radicals also combine. Also, probably due to the competition for adsorption between azo and formic dyes, further increase in formic acid does not significantly increase catalytic activity [51].

Therefore, its excessive presence prevents the formation of hydroxyl radicals and efficiency is reduced. On the other hand, due to the smaller surface area in CFSWM, more hole scavenger values are required than CFSFM to form electron–hole pairs.

3.4 *Proposed mechanism of the decolorization process*

Based on the experiment results, the mechanism of MO adsorption-photocatalytic decolorization is proposed as follows:

$$\text{Catalyst} + \text{hv} \rightarrow e^-_{\text{conduction band}} + h^+_{\text{valence band}} \quad (7)$$

$$O_2 + e^-_{\text{conduction band}} \rightarrow O_2^{-\bullet} \quad (8)$$

$$O_2^{-\bullet} + 2H^+ + e^-_{\text{conduction band}} \rightarrow H_2O_2 \quad (9)$$

$$2H_2O + 2 h^+_{\text{valence band}} \rightarrow H_2O_2 + 2H^+ \quad (10)$$

$$H_2O_2 \rightarrow 2OH^\bullet \quad (11)$$

$$h^+_{\text{valence band}}/OH^\bullet + MO + HCOO^- \\ \rightarrow \text{decolorization product } (CO_2, NO_3^-, H_2O) \quad (12)$$

Metal nanoparticles, due to the bandwidth gap of semiconductors, are used to increase adsorption-photocatalytic efficiency to increase electron hole separation, surface charge transfer and light excitation [22]. It is most probable that when a photocatalyst is exposed to ultraviolet light, an electron is excited from the capacitor layer to the conduction band, resulting in the production of an electron–hole pair [2]. This electron–hole pair reacts with the species present on the catalyst surface. In most cases, the capacitive bond hole reacts easily with the H_2O surface bond and produces a hydroxyl radical. In addition, the conductive electron reacts with oxygen to produce a superoxide radical oxygen anion. Reactions 2–5 prevent the recombination of electrons and holes formed in the first stage. $OH^\bullet$ and $O_2^{-\bullet}$ produced degrade MO.

3.5 *Process optimization*

The numerical optimization of the software using desirability approach was employed to find the specific points that maximize the adsorption-photocatalytic decolorization process. The optimum conditions for the maximum adsorption-photocatalytic decolorization efficiency for CFSFM were found as follows: catalyst concentration = 1.5 mg ml^{-1}, initial concentration of MO = 400 mg l^{-1}, formic acid concentration = 0.15% (v/v), and pH = 5, contact time = 7.5 min, speed = 300 rpm. Whereas for CFSWM the optimum conditions were as follows: catalyst concentration = 1 mg ml^{-1}, initial concentration of MO = 400 mg l^{-1}, formic acid concentration = 0.2% (v/v), and pH = 3, contact time = 10 min, speed = 400 rpm (supplementary figures S3 and S4). Finally, the results of the study showed that the studied

nanocomposites have a higher ability to degrade MO, which is probably due to the adsorption and simultaneous catalytic properties of nanocomposites. Theoretically, the adsorption-photocatalytic degradation efficiency was 100.3 ± 1.1 for CFSFM and the experimental value was 99.2 ± 0.1. For CFSWM, the predicted value and the experimental value were 92.7 ± 1.9 and 86.7 ± 1.0, respectively. It is clear that for both CFSFM and CFSWM, the predicted values are in good agreement with the experimental values under optimal conditions.

3.6 Adsorption isotherms

Langmuir, Freundlich and Temkin isotherms were used to evaluate the performance of the adsorbents studied. The linear isotherm models are listed in the following equations [52]:

Langmuir:

$$\frac{c_e}{q_e} = \frac{c_e}{q_m} + \frac{1}{q_m b} \tag{13}$$

$$R_l = \frac{1}{1 + bC_0} \tag{14}$$

Freundlich:

$$\log q_e = \log k_f + \frac{1}{n} \log C_e \tag{15}$$

Temkin:

$$Q_e = B_t \ln A_t + B_t \ln C_e \tag{16}$$

$$B = \frac{RT}{b_t} \text{ and } A = \frac{RT}{b_t} \ln k_{temkin} \tag{17}$$

where C_e is the concentration of solute aqueous in equilibrium (mg ml^{-1}), q_m the maximum dye adsorption capacity (mg g^{-1}), b the constant of Langmuir model that describes the binding energy, R_L determines the type of absorption, K_f and n are the constants of the Freundlich model, A_T (1 g^{-1}) and b_T (kJ mol^{-1}) are the constants of the Temkin model, R the global constant of gases, and T is the absolute temperature (K) [37,53].

The experiments were carried out by varying the initial MO concentrations for CFSFM (50–1000 mg l^{-1}) and CFSWM (100–1500 mg l^{-1}) at temperatures of 25°C and in optimal conditions of the adsorption isotherms.

As shown in supplementary figure S5a and b, the adsorption capacity of nanocomposite is sharply increased to reach a plateau trend, indicating that its surface can be saturated sufficiently high by dye molecules at the initial MO concentration, while its capacity for the higher MO concentration is higher.

The results showed that the laboratory data were better described by the Langmuir isotherm with an R^2 value of 0.981 and 0.992 for CFSFM and CFSWM, respectively. The adsorption capacity of the Langmuir isotherm model

was 1666.6 and 1111.1 mg g^{-1} for CFSFM and CFSWM, respectively, which indicates the high efficiency of the nanocomposite. Also, the high adsorption capacity of CFSFM can be attributed to its specific surface area (57.1 m^2 g^{-1}) and very high MnO$_2$ groups. The fact that the laboratory data were more consistent with the Langmuir model is due to the homogeneous distribution of active sites on the nanocomposite surface, because the Langmuir equation is based on the assumption that the substrate surface is homogeneous [54]. This means that there is MO monolayer coverage at the nanocomposite level. Since light transmission is an important factor in influencing the absorption-photocatalytic activity, a single layer coating may be useful for light absorption and degradation of the absorbed MO, compared to a multilayer coating [55]. In fact, all adsorption sites are equivalent and the adsorbed molecules do not interact with each other [56]. According to table 4, the value of R_L parameter was determined in the range 0.981 and 0.992 for CFSFM and CFSWM, respectively. So adsorption-photocatalytic decolorization by the prepared nanocomposite is described as favourable [53]. The value of the parameter n in the Freundlich isotherm, which is greater than one, indicates the suitability of the decolorization process. A and b_T constants and correlation coefficient R^2 Temkin isotherm model are listed in table 4. Therefore, the adsorption of MO to the adsorbent is characterized by a high amount of bonding energy. Also, the adsorption potential of B Temkin for the nanocomposites was determined to be 116.0 and 239.2 kJ mol^{-1} for CFSFM and CFSWM, respectively, which indicates the formation of a strong bond between MO molecules and the nanocomposite surface.

Table 4. Calculated constants of isotherm models.

Models	Parameters	CFSFM	CFSWM
Langmuir	q_m (mg g^{-1})	1666.6	1111.1
	b	0.048	0.01
	R_l	0.7	0.51
	R^2	0.981	0.992
Freundlich	$1/n$	0.504	0.607
	n	1.98	1.64
	K_f (mg g^{-1})	100.0	29.0
	R^2	0.837	0.969
Temkin	A_T (l g^{-1})	2.859	0.120
	b_T (kJ mol^{-1})	0.0209	0.0101
	B	116.0	239.2
	R^2	0.974	0.945

Experimental conditions for CFSFM: pH = 5, dose = 1.5 mg ml^{-1}, HS = 0.15%, time = 7.5 min under UV irradiation, speed = 300 rpm, C_i (ppm) = 50–600 ppm. Experimental conditions for CFSWM: pH = 3, dose = 1 mg ml^{-1}, HS = 0.2%, time = 10 min under UV irradiation, speed = 400 rpm, C_i (ppm) = 50–1500 ppm.

3.7 Kinetic study

One of the important factors influencing the design of adsorption-photocatalytic decolorization system is the prediction of reaction kinetics, which are important for us due to the mechanisms affecting this process. Kinetic adsorption models can evaluate the degradation process path and the process speed control mechanism. Kinetic data were analysed using some of the known kinetic models described in table 5. The linear form of the equation is as follows [57]:

Pseudo-first-order

$$\log(q_{e-}q_t) = \log q_e - \frac{k_1 t}{2.303} \tag{18}$$

Pseudo-second-order

$$\frac{t}{q_t} = \frac{1}{(k_2 q_e^2)} + \frac{1}{q_e} \tag{19}$$

where q_t (mg g^{-1}) is the amount of adsorbed solute at any time t (min), q_e (mg g^{-1}) is the amount of adsorbed solute at equilibrium conditions, and k_1 (min^{-1}) is the rate constant

and k_2 (g mg^{-1} min^{-1}) is the pseudo-second-order rate constant.

It is clear from table 5 that R^2 obtained the pseudo-second-order kinetic equation ($R^2 = 1$ and $R^2 = 99.84$) for both CFSFM and CFSWM nanocomposites more than the pseudo-first-order kinetic equation ($R^2 = 0.0209$, $R^2 = 0.7899$). In addition, the q_e values calculated by the pseudo-second-order model (263.15 mg g^{-1} for CFSFM and 357.14 mg g^{-1} for CFSWM) were obtained according to the experimental values (263.8 mg g^{-1} for CFSFM and 346.24 mg g^{-1} for CFSWM). The results indicate that the adsorption kinetics follow a pseudo-second-order model. It was clear that 88.8% of the dye molecules were rapidly adsorbed at the CFSFM after 2 min and the solution was equilibrated after 4 min. Also 75.75% of the dye molecules were adsorbed at the CFSWM after 3 min, and after 10 min equilibration was achieved. In this case, 98.9 and 86.56% of MO are absorbed, respectively. It is noteworthy that the reason for the increase in CFSFM and CFSWM adsorption probably arises not only from the compounds resulting from π–π conjugation between MO and its aromatic regions with the nanocomposite, but also from the electrostatic attraction of the MO and MnO$_2$ groups [54].

3.8 Thermodynamic studies

Thermodynamic studies can provide valuable information about the decolorization process and preparation for higher adsorption-photocatalytic performance. The most important thermodynamic parameters include Gibbs free energy changes (ΔG°), enthalpy (ΔH°) and entropy (ΔH°), which are calculated using the following equation [58].

$$\Delta G^\circ = -RT \ln K_L \tag{20}$$

The findings confirm that due to $\Delta H^o < 0$, the decolorization process is exothermic. Increasing the temperature also leads to an increase in the adsorption level to some extent, which is proportional to the ΔH^o results [59]. Also, ΔS°

Table 5. Parameters of adsorption-photocatalytic decolorization kinetic models of MO.

Kinetic	Parameters	CFSFM	CFSWM
Pseudo-first order	q_e (mg g^{-1})	95.5	326.58
	k_1 (g mg^{-1} min^{-1})	–0.018	–0.0826
	R^2	0.0209	0.7899
Pseudo-second order	q_e (mg g^{-1})	263.15	357.14
	k_2 (g mg^{-1} min^{-1})	0.0481	0.00522
	R^2	1	0.9984

Experimental conditions for CFSFM: pH = 5, dose = 1.5 mg ml^{-1}, HS = 0.15%, time = 0–60 min under UV irradiation, speed = 300 rpm, C_i (ppm) = 400 ppm. Experimental conditions for CFSWM: pH = 3, dose = 1 mg ml^{-1}, HS = 0.2%, time = 0–60 min under UV irradiation, speed = 400 rpm, C_i (ppm) = 400 ppm.

Table 6. Thermodynamic parameters for MO adsorption-photocatalytic decolorization by nanocomposites CFSFM and CFSWM on different temperatures.

Nanocomposite	T (K)	ΔG° (J mol^{-1})	ΔS° (J K^{-1} mol^{-1})	ΔH° (J mol^{-1})
CFSFM	298	– 10566.634	22.78	– 3930.4
	305	– 11021.736		
	318	– 11167.394		
	328	– 11450.960		
	338	– 11786.356		
	348	– 11672.295		
CFSWM	298	– 3967.34	0.6568	– 3878.56
	305	– 4234.83		
	318	– 4091.77		
	328	– 3993.32		
	338	– 4244.51		
	348	– 4011.38		

values indicate the value of irregularities in the solid and soluble surface during the adsorption-photocatalytic decolorization process. Considering $\Delta G° < 0$ values for both CFSFM and CFSWM nanocomposites in the studied temperature range, the adsorption-photocatalytic decolorization process is irreversible and spontaneous, and shows that the reaction is easily carried out at higher temperatures. In addition, the chemical or physical nature of the adsorption process can be determined with the help of $\Delta G°$. In general, for physical adsorption, the Gibbs free energy variation is in the range of 0 to –20 kJ mol^{-1}, while the amount of change in Gibbs free energy for chemical adsorption varies between – 80 and – 400 kJ mol^{-1} [60]. According to the values shown in table 6, the adsorption process of MO is chemical. This type of adsorption is the result of chemical bonds between the adsorbent and the adsorbent. The effect of temperature increase can be expressed by the possible effect of ultraviolet light on the total pore capacity and adsorption

porosity, which increases the diffusion of MO on the outer surface in addition to the inner pores of the nanocomposite. Also, increasing the temperature of aqueous solutions creates more bubbles formed in the liquid phase and improves the dispersion of nanocomposite-MO. As a result, it accelerates the rate of MO degradation. For a better understanding, the thermodynamic parameters of the MO adsorption-photocatalytic decolorization process at different temperatures of 293, 308, 316, 327, 338 and 348 K are summarized in table 6.

4. Real samples

In order to study the applicability of adsorption-photocatalytic decolorization by two composites CFSFM and CFSWM, on two real samples, ground water and industrial town effluent, at spiked concentrations of 200–400 ppm of MO dye. The dye degradation efficiencies by both CFSFM and CFSWM were examined. As shown in figure 8a and b, the dye concentration was significantly reduced after applying the optimal conditions using both nanocomposites. However, the residual concentration of MO after adsorption-photocatalytic process for CFSFM was lower than CFSWM. Since the residual dye concentrations were less than the standard value for discharge, the studied nanocomposite substrates have a very good performance for the treatment of MO dye solutions from water and wastewater media.
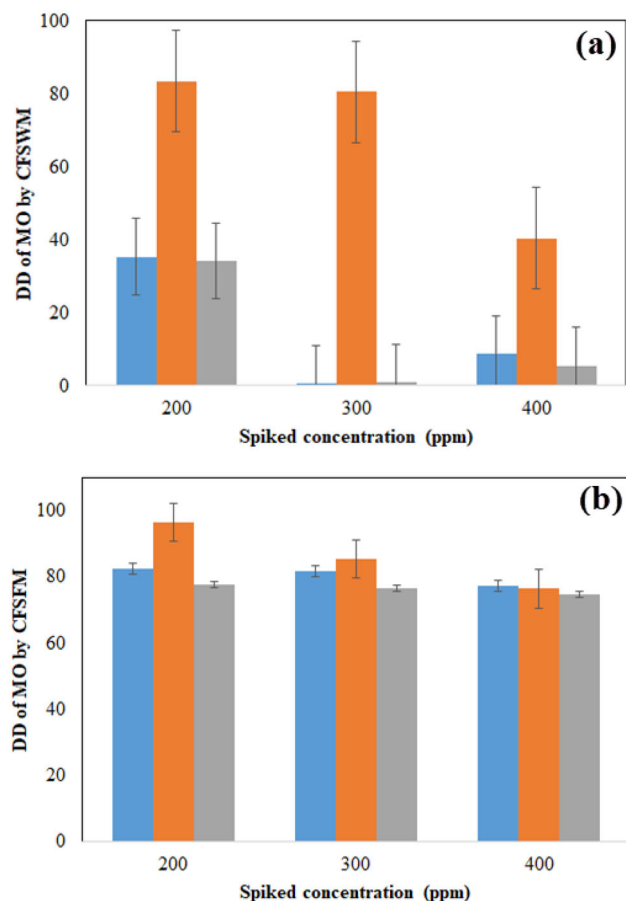
5. Conclusions

Because of the specific nature of some of the waste from industries, the possibility of direct biological treatment is not possible, therefore, new methods such as advanced oxidation processes for the treatment of these pollutants are proposed. These methods are based on the production of highly active species such as hydroxyl radicals that can rapidly oxidize a wide range of organic pollutants, including MO. Among the advanced oxidation processes, heterogeneous adsorption-photocatalysts presented satisfactory results in the degradation of resistant and toxic organic materials and the production of materials with less toxicity and biodegradability. Among different nanocomposites, CFSFM and CFSWM were used for adsorption-photocatalytic decolorization of MO in this study due to its high adsorption-photocatalytic activity, non-toxicity, chemical stability and cost-effectiveness. Understanding the effect of various factors on efficiency of the adsorption-photocatalytic decolorization process is of the utmost importance in the design of this process for industrial scale purification. The effect of factors that can be effective was investigated and high decolorization efficiency was achieved under

Figure 8. Percentage of real sample decolorization. (**a**) CFSFM nanocomposite, experimental conditions: pH = 5, dose = 1.5 mg ml^{-1}, HS = 0.15%, time = 7.5 min UV, speed = 300 rpm, C_i (ppm) = 200–400 ppm. (**b**) CFSWM nanocomposite, experimental conditions: pH = 3, dose = 1mg ml^{-1}, HS = 0.2%, time = 10 min UV, speed = 400 rpm, C_i (ppm) = 200–400 ppm.

optimal conditions. According to the results, this method can be used as an efficient method for the treatment of effluents containing dyes.

Acknowledgement

References

[1] Saemian T, Gharagozlou M, Hossaini Sadr M and Naghibi S 2020 *J. Inorg. Organomet. Polym. Mater.* **30** 23472

[2] Xiao L, Sun W, Zhou X, Cai Z and Hu F 2018 *Vacuum* **156** 2913

[3] Revathi J, Abel M J, Archana V, Sumithra T, Thiruneelakandan R and Joseph Prince J 2020 *Phys. B Condens. Matter* **587** 412136

[4] Cai B, Feng J-F, Peng Q-Y, Zhao H-F, Miao Y-C and Pan H 2020 *J. Hazard. Mater.* **392** 1222795

[5] Nguyen C H, Fu C C and Juang R S 2018 *J. Clean. Prod.* **202** 413

[6] Dhir R 2020 *Chem. Phys. Lett.* **746** 1373027

[7] Gomathi Devi L, Girish Kumar S, Mohan Reddy K and Munikrishnappa C 2009 *J. Hazard. Mater.* **164** 459

[8] Bahrudin N N, Nawi M A and Zainal Z 2020 *Int. J. Biol. Macromol.* **165** 24629

[9] Smith Y R, Kar A and Subramanian V 2009 *Ind. Eng. Chem. Res.* **48** 10268

[10] Yuvaraja G, Chen D Y, Pathak J L, Long J, Subbaiah M V, Wen J C et al 2020 *Int. J. Biol. Macromol.* **146** 1100

[11] Youssef N A, Shaban S A, Ibrahim F A and Mahmoud A S 2016 *Egypt. J. Pet.* **25** 317

[12] Yu H, Li Y, Zhao M, Dong H, Yu H, Zhan S et al 2015 *Catal. Today* **258** 156

[13] Semiz L 2020 *J. Inst. Sci. Technol.* **98** 32814

[14] Wang J C, Lou H H, Xu Z H, Cui C X, Li Z J, Jiang K et al 2018 *J. Hazard. Mater.* **360** 356

[15] Tseng W J and De Lin R 2014 *J. Colloid Interface Sci.* **428** 9516

[16] Hao W, Xi Y, Hu J, Wang T, Du Y and Wang X L 2012 *J. Appl. Phys.* **111** 07B301

[17] Yang Q, Song H, Li Y, Pan Z, Dong M, Chen F et al 2017 *J. Mol. Liq.* **234** 1818

[18] Wang N, Pang H, Peng H, Li G and Chen X 2009 *Cryst. Res. Technol.* **44** 1230

[19] Hui J, Pestana C J, Caux M, Gunaratne H Q N, Edwards C, Robertson P K J et al 2021 *J. Photochem. Photobiol. A Chem.* **405** 112935

[20] Ren C, Yang B, Wu M, Xu J, Fu Z, lv Y et al 2010 *J. Hazard. Mater.* **182** 123

[21] Pargoletti E, Pifferi V, Falciola L, Facchinetti G, Re Depaolini A, Davoli E et al 2019 *Appl. Surf. Sci.* **472** 118

[22] Osgouei M S, Khatamian M and Kakili H 2020 *Mater. Chem. Phys.* **239** 122108

[23] Sun Y G, Truong T T, Liu Y Z and Hu Y X 2015 *Chin. Chem. Lett.* **26** 233

[24] Xia H, Feng J, Wang H, Lai M O and Lu L 2010 *J. Power Sources* **195** 441025

[25] Sun F, He J, Wu P, Zeng Q, Liu C and Jiang W 2020 *Chem. Eng. J.* **397** 12539726

[26] Wang F, Dai H, Deng J, Bai G, Ji K and Liu Y 2012 *Environ. Sci. Technol.* **46** 403427

[27] Das S, Samanta A and Jana S 2017 *ACS Sustain. Chem. Eng.* **5** 9086

[28] Yang Y, Wang G, Deng Q, Ng D H L and Zhao H 2014 *ACS Appl. Mater. Interfaces* **6** 300829

[29] Anh Tran V, Khoa Phung T, Le Thuan V, Ky Vo T, Tai Nguyen T, Anh Nga Nguyen T et al 2021 *Mater. Lett.* **284** 12890230

[30] Li L, Chu Y, Liu Y and Dong L 2007 *Mater. Lett.* **61** 1609

[31] Zhang Y, Xu Q, Zhang S, Liu J, Zhou J, Xu H et al 2013 *Sep. Purif. Technol.* **116** 391

[32] Wang Y, Fu Y, Wu X, Zhang W, Wang Q and Li J 2017 *Ceram. Int.* **43** 1136733

[33] Xiang B, Ling D, Lou H and Gu H 2017 *J. Hazard. Mater.* **325** 178

[34] Lowell S, Shields J E, Thomas M A and Thommes M 2005 *Characterization of porous solids and powders: surface area, pore size, and density* (Netherlands: Springer)

[35] Qi C, Zhu Y J, Wu C T, Sun T W, Jiang Y Y, Zhang Y G et al 2016 *RSC Adv.* **6** 968636

[36] Maroudas A, Pandis P K, Chatzopoulou A, Davellas L R, Sourkouni G and Argirusis C 2021 *Ultrason. Sonochem.* **71** 105367

[37] Tanhaei B, Ayati A, Iakovleva E and Sillanpää M 2020 *Int. J. Biol. Macromol.* **164** 362138

[38] Du Y, Wang L, Wang J, Zheng G, Wu J and Dai H 2015 *J. Environ. Sci. (China)* **29** 7139

[39] Montgomery D 2012 *Design and analysis of experiments* (United States: Wiley)

[40] Soltani R D C, Rezaee A, Khataee A R and Safari M 2014 *J. Ind. Eng. Chem.* **20** 186141

[41] Abbas-Shiroodi Z, Sadeghi M T and Baradaran S 2021 *Ultrason. Sonochem.* **71** 10538642

[42] Zeraatkar Moghaddam A, Esmaeilkhanian E and Shakourian-Fard M 2019 *Int. J. Biol. Macromol.* **128** 6143

[43] Khataee A R, Zarei M and Asl S K 2010 *J. Electroanal. Chem.* **648** 14344

[44] Antonopoulou M, Giannakas A and Konstantinou I 2012 *Int. J. Photoenergy* **2012** 145

[45] Murray L, Mason R L, Gunst R F and Hess J L 1990 Statistical *design and analysis of experiments: with applications to engineering and science* (United States: Wiley) p 46

[46] Zuorro A and Lavecchia R 2014 *Desalin. Water Treat.* **52** 1571

[47] Chatterjee D and Dasgupta S 2005 *J. Photochem. Photobiol. C Photochem. Rev.* **6** 186

[48] Doudrick K, Yang T, Hristovski K and Westerhoff P 2013 *Appl. Catal. B Environ.* **136–137** 4049

[49] Tan T, Beydoun D and Amal R 2003 *J. Photochem. Photobiol. A Chem.* **159** 27350

[50] Ma M, Yang Y, Chen Y, Ma Y, Lyu P, Cui A et al 2021 *J. Alloys Compd.* **861** 15825651

[51] Rengaraj S and Li X Z 2007 *Chemosphere* **66** 93052

[52] Dada A O, Olakekan A P, Olatunya A M and Dada O 2012 *J. Appl. Chem.* **3** 3853

[53] Ren Y, Abbood H A, He F, Peng H and Huang K 2013 *Chem. Eng. J.* **226** 30054

[54] Zhang L, Li H, Liu Y, Tian Z, Yang B, Sun Z *et al* 2014 *RSC Adv.* **4** 4870355

[55] Chen F, Liu Z, Liu Y, Fang P and Dai Y 2013 *Chem. Eng. J.* **221** 28356

[56] Chen F, Fang P, Gao Y, Liu Z, Liu Y and Dai Y 2012 *Chem. Eng. J.* **204** 107

[57] Zhang Z, Wang G, Li W, Zhang L, Chen T and Ding L 2020 *Colloids Surfaces A Physicochem. Eng. Asp.* **601** 12503458

[58] Azari A, Mahmoudian M H, Niari M H, Eş I, Dehganifard E, Kiani A *et al* 2019 *Microchem. J.* **150** 1041 4459

[59] Choudhary B and Paul D 2018 *J. Environ. Chem. Eng.* **6** 2335

[60] Greluk M and Hubicki Z 2010 *Chem. Eng. J.* **162** 919